AFRL-RX-WP-TP-2008-4351

MICROSTRUCTURE EVOLUTION DURING WARM WORKING OF Ti-6Al-4V WITH A COLONY ALPHA MICROSTRUCTURE (PREPRINT)

S. Mironov, M. Murzinova, S. Zherebtsov, G.A. Salishchev, and S.L. Semiatin

Metals Branch
Metals, Ceramics, and NDE Division

SEPTEMBER 2008

AIR FORCE RESEARCH LABORATORY
MATERIALS AND MANUFACTURING DIRECTORATE
WRIGHT-PATTERSON AIR FORCE BASE, OH 45433-7750
AIR FORCE MATERIEL COMMAND
UNITED STATES AIR FORCE

REPORT DOCUMENTATION PAGE

Form Approved
OMB No. 0704-0188

1. REPORT DATE *(DD-MM-YY)*	2. REPORT TYPE	3. DATES COVERED *(From - To)*
September 2008	Journal Article Preprint	

4. TITLE AND SUBTITLE

MICROSTRUCTURE EVOLUTION DURING WARM WORKING OF Ti-6Al-4V WITH A COLONY ALPHA MICROSTRUCTURE (PREPRINT)

5a. CONTRACT NUMBER
In-house

5b. GRANT NUMBER

5c. PROGRAM ELEMENT NUMBER
62102F

6. AUTHOR(S)

S. Mironov (Tohoku University)
M. Murzinova (Russian Academy of Science)
S. Zherebtsov and G.A. Salishchev (Belgorod State University)
S.L. Semiatin (AFRL/RXLMP)

5d. PROJECT NUMBER
4347

5e. TASK NUMBER
RG

5f. WORK UNIT NUMBER
M02R2000

7. PERFORMING ORGANIZATION NAME(S) AND ADDRESS(ES)

Tohoku University
Russian Academy of Science
Belgorod State University

Metals Branch (AFRL/RXLMP)
Metals, Ceramics, and NDE Division
Materials and Manufacturing Directorate
Wright-Patterson Air Force Base, OH 45433-7750
Air Force Materiel Command, United States Air Force

8. PERFORMING ORGANIZATION REPORT NUMBER
AFRL-RX-WP-TP-2008-4351

9. SPONSORING/MONITORING AGENCY NAME(S) AND ADDRESS(ES)

Air Force Research Laboratory
Materials and Manufacturing Directorate
Wright-Patterson Air Force Base, OH 45433-7750
Air Force Materiel Command
United States Air Force

10. SPONSORING/MONITORING AGENCY ACRONYM(S)
AFRL/RXLMP

11. SPONSORING/MONITORING AGENCY REPORT NUMBER(S)
AFRL-RX-WP-TP-2008-4351

12. DISTRIBUTION/AVAILABILITY STATEMENT

Approved for public release; distribution unlimited.

13. SUPPLEMENTARY NOTES

Journal article submitted to the *Acta Materialia*. PAO Case Number: WPAFB 08-5309; Clearance Date: 04 Sep 2008. The U.S. Government is joint author of this work and has the right to use, modify, reproduce, release, perform, display, or disclose the work. Paper contains color.

14. ABSTRACT

A high-resolution electron-backscatter-diffraction (EBSD) technique was employed to investigate microstructure evolution during warm working of Ti-6Al-4V with a colony alpha microstructure. Particular emphasis was paid to the specific mechanisms governing this process. Microstructure development was found to be driven mainly by the geometrical requirements of the imposed strain and by the kinking of alpha lamellae. For the most part, the lamellar microstructure was surprisingly stable during straining with limited globularization observed only in kinked alpha colonies. The kinking process was shown to be closely linked with the development of shear bands within the colonies. These observations suggest that changes in strain path may be beneficial in promoting globularization during warm working.

15. SUBJECT TERMS

titanium alloys, warm working, microstructure, electron backscatter diffraction

16. SECURITY CLASSIFICATION OF:			17. LIMITATION OF ABSTRACT:	18. NUMBER OF PAGES	19a. NAME OF RESPONSIBLE PERSON (Monitor)
a. REPORT	b. ABSTRACT	c. THIS PAGE			Sheldon L. Semiatin
Unclassified	Unclassified	Unclassified	SAR	30	19b. TELEPHONE NUMBER *(Include Area Code)* N/A

Standard Form 298 (Rev. 8-98)
Prescribed by ANSI Std. Z39-18

Microstructure Evolution during Warm Working of Ti-6Al-4V with a Colony-α Microstructure

S. Mironov[1], M. Murzinova[2], S. Zherebtsov[3], G.A. Salishchev[3], and S.L. Semiatin[4]

[1]Department of Materials Processing, Graduate School of Engineering,
Tohoku University, 6-6-02 Aramaki-aza-Aoba, Sendai 980-8579, Japan
[2]Institute for Metals Superplasticity Problems, Russian Academy of Science, 39 Khalturin Str., Ufa, 450001, Russia
[3]Centre of Nanostructured Materials and Nanotechnologies, Belgorod State University,
85 Pobeda Str., Belgorod, 308015, Russia
[4]Air Force Research Laboratory, Materials and Manufacturing Directorate, AFRL/RXLM,
Wright-Patterson AFB, OH 45433-7817, USA

A high-resolution electron-backscatter-diffraction (EBSD) technique was employed to investigate microstructure evolution during warm working of Ti-6Al-4V with a colony-α microstructure. Particular emphasis was paid to the specific mechanisms governing this process. Microstructure development was found to be driven mainly by the geometrical requirements of the imposed strain and by the kinking of α lamellae. For the most part, the lamellar microstructure was surprisingly stable during straining with limited globularization observed only in kinked α colonies. The kinking process was shown to be closely linked with the development of shear bands within the colonies. These observations suggest that changes in strain path may be beneficial in promoting globularization during warm working.

Keywords: Titanium alloys; Warm working; Microstructure; Electron backscatter diffraction

1. INTRODUCTION

The two-phase α/β titanium alloy Ti-6Al-4V is the backbone of titanium industry especially for aerospace applications. This material is usually produced by an ingot-metallurgy route comprising a series of steps each of which has specific microstructural goals. Following casting, ingots are typically hot worked and heat treated above the β transus (temperature at which α + β → β) in order to eliminate casting inhomogeneities. Depending on the cooling rate following β processing, a variety of so-called transformed-β microstructures, ranging from those comprising coarse lamellar colonies to those consisting of very fine, acicular martensitic α, can be formed. Although such microstructures may promote resistance to fracture and high-temperature creep, a low-aspect ratio (so-called “globular”) microstructure is often desirable for applications requiring optimal strength or ductility. In this regard, lamellar microstructures are typically broken down to produce the desired globular ones via subtransus processing. This technological stage represents both the most difficult step from a workability standpoint as well as the most important with regard to final shaping and service.

Because of its great technological importance, the globularization process has been studied for many years. The majority of this research has focused on globularization at relatively

high temperatures (800-950°C) [1 - 6]. In this prior work, it was established that there are generally two ways by which lamellae globularize during (and following) hot deformation [1]. Both involve the formation of boundaries across individual α lamellae and the subsequent diffusional penetration of the β phase along these boundaries, finally leading to break up of the lamellar α microstructure. In one case, the α/α grain boundaries originate from a recrystallization process, whereas in the second they are formed by deformation-induced intense, localized shear across the α lamellae.

Recent work has shown that globularization at lower temperatures can lead to the formation of a finer $\alpha+\beta$ microstructure compared to that achieved at higher temperatures [7, 8]. In fact, a submicrocrystalline structure has been produced by warm working at a temperature of ~550°C [8]. Such refined microstructures may impart significantly higher strength at service temperatures and noticeably improved ductility at higher temperatures. Microstructure refinement in Ti-6Al-4V is therefore of considerable commercial interest. In addition, the physical basis of the globularization process at low temperatures is not clear, and the phenomenon is thus of substantial scientific interest as well.

Limited observations of Ti-6Al-4V have suggested several important features of the evolution of microstructure during deformation at low temperatures (550-700°C) [7 - 9]. First, the majority of the α laths tend to become aligned in the principal direction of material flow, whereas some α colonies become kinked [9]. On a finer scale, the α laths become subdivided with increasing strain leading to the formation of rows of relatively low-aspect ratio α particles/grains (or subgrains); details of this process are not clear, however [9]. Nevertheless, it has been demonstrated that globularization kinetics are significantly influenced by strain path. For a fixed strain path (e.g., extrusion), the lamellae microstructure is surprisingly stable, constituting ~60 volume percent of the material after true strains as large as 1.8 [9]. On the other hand, a change in strain path (e.g., via “abc”-deformation) promotes the formation of a relatively homogeneous globular microstructure after true strains of ~ 3 [8].

Prior research has provided broad insight into the globularization process at relatively low (warm-working) temperatures. However, these efforts have concentrated primarily on *final* microstructure with relatively little attention on the detailed mechanism of how microstructure evolves with deformation. The object of the present work, therefore, was to delineate the details of the mechanism by which globularization occurs during warm working of α/β titanium alloys with a lamellar perform microstructure. For this purpose, scanning-electron-microscopy (SEM) and electron-backscatter-diffraction (EBSD) were performed on Ti-6Al-4V samples deformed to different strain levels.

2. MATERIAL AND EXPERIMENTAL PROCEDURES

The material used in the present investigation was commercial grade Ti-6Al-4V whose measured composition (in wt. pct) was 6.3 aluminum, 4.1 vanadium, 0.18 iron, 0.03 silicon, 0.002 zirconium, 0.01 carbon, 0.18 oxygen, and 0.01 nitrogen, with the balance being titanium. The β transus for this material was approximately 995°C. The material was supplied as 18-mm

diameter hot-rolled bar with a duplex microstructure consisting of primary α in a transformed-β matrix. The as-received bar was heat treated using a cycle comprising 955°C/15 min + 1010°C/15 min + furnace cool to 800°C/soak for 20 min + controlled furnace cool (at a rate of 2°C/min) to 600°C/soak for 2 h + water quench. By this means a colony-α preform microstructure was developed.

Cylindrical specimens measuring 12-mm height and 8 mm diameter were machined from the heat-treated bar. The specimens were uniaxially compressed to a height reduction of 25, 50, or 70 pct. at 600°C and an initial strain rate of 10^{-3} s^{-1} using a Schenk universal testing machine. After deformation, all specimens were water quenched to preserve the as-deformed microstructure. A sample was also heated to the deformation temperature, given an identical soak, and water quenched to determine the undeformed microstructure. Following deformation, each specimen was sectioned axially and prepared for SEM and EBSD. For SEM observations, the specimens were mechanically polished, electro-polished in an 80:20 pct. acetic anhydride: perchloric acid solution at ~15°C using a DC power supply operated at 70V, and etched with Kroll's reagent (95% H_2O, 3% HNO_3, 2% HF). For EBSD, samples were mechanically polished followed by electropolishing in a solution of 5 pct. perchloric acid, 35 pct. butanol, and 60 pct. methanol at approximately -35°C with an applied potential of 40V.

All microstructure observations focused on the central (most-highly deformed) region of the compression specimens; all SEM micrographs and EBSD scans were taken such that the compression direction was vertical. SEM studies were carried out using a JEOL JSM-6400. High resolution EBSD analysis was conducted in a Hitachi S-4300SE FEG SEM equipped with TSL OIM™ software. Orientation mapping involved automated beam control using a triangular scanning grid; step sizes were 0.1 - 1 μm. For each diffraction pattern, nine Kikuchi bands were used for indexing to minimize errors. In this manner, EBSD maps comprising ~400,000 points were obtained. The *average* confidence index (CI) for each EBSD map ranged from 0.66 to 0.12. By comparison, experiments on face-centered cubic (fcc) materials have shown that the fraction of correctly indexed patterns with CI's greater than 0.1 is 95 pct. [10]. To obtain a more reliable picture of microstructure evolution, small grains comprising three or fewer pixels were automatically removed from the maps using the grain-dilation function in the TSL software. To eliminate spurious boundaries caused by orientation noise, a lower-limit boundary misorientation cutoff of 2° was used. All misorientation angles quoted below are relative to the rotation axis with the minimum misorientation. A misorientation of 15° was used to separate low-angle boundaries (LABs) from high-angle boundaries (HABs).

3. RESULTS and DISCUSSION

3.1 General observations of microstructure evolution

General trends of microstructure evolution during warm deformation are summarized in Figs. 1 and 2. The effect of strain on microstructural morphology is illustrated by the SEM micrographs in Fig. 1; here, the hexagonal close-packed (hcp) α phase is dark, and the body-centered cubic (bcc) β phase is the lighter constituent. The material quenched immediately

prior to deformation had a ”classical” transformed colony-α microstructure consisting of three micro-constituents: lamellar/basketweave α colonies with 2-μm thick α platelets, layers of α at the prior-β grain boundaries, and thin (~ 0.6 μm) β layers separating the α lamellae (Fig. 1a). The β volume fraction was measured to be ~ 18 ± 1 pct.

Microstructure evolution as a function of strain was found to be significantly influenced by the orientation of specific α colonies with respect to loading axis. If the angle between the α lamellae and compression direction was relatively small, the α laths became kinked (e.g., circled areas in Figs. 1b, c). Otherwise, the α lamellae rotated with strain, eventually becoming aligned with a direction approximately perpendicular to the loading axis (Fig. 2a). Such alignment of the α laths gradually eliminated the morphological differences between neighboring α colonies and resulted in the formation of a relatively homogeneous microstructure (Figs. 1c-d). This behavior is well documented for Ti-6Al-4V deformed at relatively high temperatures [3, 6]. The primary difference for the present case involving warm working was that the β layers generally did not break up and were continuous in nature even at large strains (e.g., high-magnification inserts in Figs. 1b-d). These observations indicate that the globularization process is noticeably retarded. By comparison, dynamic globularization during hot working is typically completed at a height reduction of ~80 pct. [3].

The effect of strain on the average thickness of the α and β laths is shown in Fig. 2b. The measured thickness of the α lamellae appeared to decrease with strain. It should be pointed out, however, that the measurements in Fig. 2b may not represent the true α platelet thickness because of stereological effects. In particular, if the plane of the platelets is not normal to the sectioning plane, the actual thickness of the α lamellae would be *less* than that measured on micrographs. This effect is greatest at low strains at which the α platelets lie at arbitrary angles to the sectioning plane. In such cases, the true α platelet thickness is approximately (1/1.5) times the measured thickness [11]. By contrast, at large strains, the α platelets rotate to an orientation close to being perpendicular to the compression axis (Fig. 2a) and the sectioning plane. In such cases, an axial section might indeed give a reasonable estimate of the platelet thickness. In view of these considerations, the actual rate of the α lamellae compression is thus less than the one shown in Fig. 2b.

The results in Fig. 2b also reveal that the average thickness of the β laths appeared to undergo little change with strain. This observation appears surprising because the β phase is generally believed to be softer than the α phase, at least at hot working temperatures. The deformation behavior of the β phase in Ti-6Al-4V thus deserves further investigation.

3.2. Burgers orientation relationship between the α and β phases

An important feature of the colony-α microstructure in α/β titanium alloys such as Ti-6Al-4V is the Burgers orientation relationship (OR) between the α and β phases in which the respective close-packed planes ($\{0002\}_\alpha/\{110\}_\beta$) and close-packed directions ($<11\bar{2}0>_\alpha$ / $<111>_\beta$) are parallel. This relationship may provide easy slip transmission across α/β interfaces such that an individual α colony behaves as a single grain [12, 13]. In the present work, EBSD provided insight into the local crystallographic relationship between the α and β phases and how

it evolved with strain. To this end, orientation data for both phases were derived from high-resolution EBSD maps covering single α colonies; these data were used to construct 110 and 111 pole figures for the β phase and 0002 and $11\bar{2}0$ pole figures for the α phase (Fig. 3).

In the *undeformed* material, the (0001) plane and one of $<11\bar{2}0>$ directions of the α phase were nearly parallel to the one of the {110} planes and one of the <111> directions in this plane of the β phase, respectively (Fig. 3a). Thus, the α and β phases were indeed related by the Burgers OR. Warm plastic deformation increased the orientation spread substantially in both phases and caused significant crystallographic rotations, leading to deviations from the exact Burgers OR at 25-pct. height reduction (Fig. 3b) or elimination of it at 50-pct. reduction (Fig. 3c).

Because the β layers were very thin (~0.6 μm) and usually gave rise to diffuse Kikuchi patterns, it was difficult to ascertain whether the examples in Fig. 3 were truly representative. To provide evidence of the elimination of the OR which was more statistically reliable, the boundaries between α colonies within given beta grains were examined. In particular, due to the crystllography of the α and β phases, there are 12 possible α orientations (each satisfying the Burgers OR) that can transform from a single parent β grain; i.e., there are 6 {110} planes in a given β grain, each containing 2 <111> directions, on which an α variant/colony can form. The possible misorientations between α variants/colonies inherited from the same parent β grain are summarized in Table 1. It is seen that these misorientations are typically very specific, and their unique nature is thus indicative of the Burgers OR.

Fig. 4 shows EBSD image quality (IQ) maps in which the boundaries between the α variants for both the starting and the deformed material have been highlighted. The IQ map quantifies the sharpness of the Kikuchi pattern at each point and is similar to an SEM image with the difference that the β phase appears dark and the alpha phase light. Fig. 4a shows that the colony boundaries in the initial material formed a continuous network. Using a 5° tolerance criterion, the boundaries between the α variants accounted for ~70 pct. of the total boundary area in the α phase, thus confirming the Burgers OR between the α and β phases (Fig. 3a). After 25-pct. height reduction, the boundary network became discontinuous (Fig. 4b). This observation suggests that adjacent colonies may have rotated relative to one another producing localized flow in the boundary between them and hence loss of the OR. This process is similar to the evolution of twin misorientations in pure titanium during straining [16] and may be explained by local deformation-induced crystallographic rotation of each α colony away from its initial orientation inherited during the β-to-α phase transformation. This result supports the conclusion that the breakdown of the Burgers OR between the α and β phases began at reductions of the order of 25 pct. (Fig. 3b). In the material deformed to a height reduction of 50 to 70 pct., the inter-colony boundaries have disappeared almost completely, and only a few local boundary segments were noted (Figs. 4c, d).

3.3. Orientation spread within α colonies

The breakdown of the Burgers OR was associated with significant crystallographic rotations of the α and β phases within the α colonies. In order to provide a deeper insight into this phenomenon, orientation variations transverse and parallel to α laths were measured in EBSD

maps such as those shown in Fig. 4; typical examples of the cumulative misorientation are given in Figs. 5 and 6, respectively.

In the undeformed material (Figs. 5a and 6a), orientation variations in both the transverse and parallel directions were generally within the angular resolution of EBSD (~2°). Thus, the α laths within a given colony had essentially the same crystallographic orientation, and the orientation spread was very small. These observations were as expected and may be readily explained in terms of the Burgers OR governing the β-to-α phase transformation (Fig. 3a).

Plastic deformation gave rise to a significant orientation spread within each α colony as well as within individual α laths. The misorientation profile in the direction *transverse* to the α laths (Figs. 5b-d) showed alternating orientation changes with a "wavelength" of ~5-10 μm, a length which is comparable to the initial α lath thickness of ~2 μm. This suggests that groups of neighboring α laths rotated relative to each other, and these rotations tended to compensate each other. This trend is reminiscent of observations for deformed single-phase fcc metals [e.g., 17, 18]; for such materials, imposed deformation is accommodated by the activation of different slip systems in adjoining cell blocks [19]. The number of slip systems operating in such cell blocks is fewer than that required for uniform (isostrain) deformation, but the Mises requirement is globally satisfied on the grain scale by the overall deformation behavior of the cell blocks within a given grain [18]. Because α titanium has a limited number of independent slip systems, making the accommodation of arbitrary strains difficult, reasoning analogous to that proposed for fcc metals seems appropriate to explain the alternating nature of the orientation spread (Figs. 5b-d). Additional theoretical and experimental work is needed to verify this hypothesis, however.

It is also important to note that neighboring α laths started to rotate relative to each other at a height reduction as low as 25 pct. (Fig. 5b). At this strain level, the Burgers OR between the phases was still somewhat evident (Figs. 3b and 4b), and hence the α colonies should have behaved as a single grain [12, 13]. However, this was not the case, and thus the Burgers OR itself does not ensure homogeneous deformation within the α colonies during warm working.

EBSD profiles measured *along the length* of α laths revealed broadly increasing misorientations with distance (Figs. 6b, c, d). The misorientation profiles were typically relatively smooth, suggesting that the orientation change was continuous in nature rather than one associated with the formation of high-angle boundaries. Furthermore, the magnitude of the orientation gradient was found to increase with strain, reaching ~5°/μm at a height reduction of 70 pct. (Fig. 6d). Pantleon [19] attributed similar findings to the activation of the same set of slip systems to different degrees. The present observations may also be interpreted in terms of significant internal stress within the α laths. The internal stress appears to increase abruptly in a strain range between 25 and 50 pct height reduction (Figs. 6b, c). At this strain level, the Burgers OR is destroyed (Figs. 3b-c and 4b-c). Therefore, these two phenomena may be related.

3.4. Grain boundaries in the α phase

In order to provide fundamental insight into the globularization process, it is necessary to study the development of grain boundaries in the α phase. Representative EBSD maps showing the arrangement of low- and high-angle boundaries in the starting and deformed materials are given

in Fig. 7. In the maps, all possible α grain boundaries are shown including those between α variants/colonies as well as the boundaries within/between the α laths; LABs and HABs are depicted as red and black lines, respectively. Misorientation data derived from large EBSD maps (including several thousands of α laths each) are summarized in Fig. 8.

In the *undeformed* material, most of the boundaries were high angle in character; only sporadic LABs were found within some α colonies (Fig. 7a). The misorientation distribution was dominated by 10°, 60°, and 90° boundaries whose rotation axes were clustered near the [0001] and $<2\bar{1}\bar{1}0>$ poles (Fig. 8a). A comparison of the measured misorientations (Fig. 8a) and those predicted for the Burgers OR (Table 1) showed very close agreement. As mentioned in Section 3.2, the fraction of the boundaries between the α variants in the undeformed material was 70 pct., thus indicating that these boundaries originated primarily from the β-to-α phase transformation involving the Burgers OR. The remaining 30 pct of the α grain boundaries included some LABs and boundaries between parent β grains.

Plastic deformation dramatically increased the fraction of LABs (Figs. 7b, c, d) skewing the misorientation-angle distribution towards low-angle rotations (Figs. 8b-d). After a 25-pct. height reduction, the distribution still exhibited several misorientation peaks associated with the Burgers OR (Fig. 8b), but larger strains led to the unambiguous dominance of maxima at low misorientation angles (Figs. 8c, d). Furthermore, with increasing strain, the misorientation across some boundary segments began to reach and exceed 15°. This trend was most obvious for the sample subjected to the 70-pct. height reduction (Fig. 8d). The general deformation of the alpha colonies brought about by the imposed compressive strain also contributed to an increase in the fraction of HABs (Figs. 8b-d). It should be emphasized, however, that the deformation-induced boundaries in the EBSD maps were not located randomly within the microstructure, but were aligned primarily with the longitudinal direction separating neighboring α laths (Figs. 7b-d). In reality, neighboring α laths within an α colony have no common grain boundary in the actual microstructure because they are usually separated by a continuous layer of β, as shown in the high-magnification inserts in Figs. 1b-d. This observation may therefore be explained in terms of the low resolution of the β phase in EBSD, as mentioned above. In other words, the β phase is frequently missed during EBSD or “cleaned” during data processing. It is likely therefore that the longitudinal boundaries seen in the EBSD maps are somewhat artificial and simply reflect the orientation difference between neighboring α laths, as shown in Figs. 5b-d.

The clustering of the rotation axes near <0001> as low-angle boundaries were developed (Figs. 8b-d) is of particular interest. Because the formation of the misorientations was mainly associated with the crystallographic rotation of neighboring α laths, this finding provides insight into the nature of deformation and slip in the colony microstructure. It is generally accepted that the activity of slip system *p* rotates the crystalline lattice around the axis $w_p \parallel (b \times n)_p$, in which *b* denotes the Burgers vector magnitude, and *n* is the slip plane normal. Among the possible slip modes in α titanium (prism, basal, and pyramidal), *only* prism slip provides a lattice rotation about the [0001] direction. Thus, the proximity of the rotation axes of the grain boundaries to the [0001] pole indirectly suggests preferential activation of prism slip, which is commonly accepted

to be the dominant deformation mode in alpha titanium [21]. However, prism slip alone cannot provide the five independent slip systems necessary to accommodate an arbitrary imposed strain within each grain of a polycrystalline aggregate. Hence, it is likely that prism slip was augmented by the activation of other slip and/or twinning systems. In this regard, there is some evidence of twinning in the misorientation-axis distributions (Figs. 8c-d). The rotation axes of the 85-90^{o} boundaries near $<2\bar{1}\,\bar{1}0>$ and $<10\bar{1}0>$ may be attributed to $\{10\bar{1}2\}$ and $\{11\bar{2}3\}$ twinning [15]. An example of a possible $\{11\bar{2}3\}$ twin is indicated by the arrow in Fig 7c. It should be noted, nevertheless, that twin identification requires determination of not only the grain-boundary misorientation but also the twin boundary plane. Misorientation data are routinely provided by EBSD but grain boundary planes cannot be measured due to the two-dimensional nature of EBSD maps. Hence, the present conclusion should be regarded as preliminary.

3.5. Kinking of α colonies

The grain-boundary maps in Figs. 7b-d showed that the α laths contained only a limited number of transverse boundaries, and most of these were low angle in nature. This finding underscores the observation that the rate of dynamic globularization of the α phase at warm-working temperatures was much slower than in the hot-working regime. In fact, only a small fraction of globularized microstructure was found in the deformed material (Fig. 7c).

The globularized regions were typically found in areas in which the colonies had formed kinks. Hence, high-resolution EBSD was applied to gain insight into the details of the kinking process. To obtain maximum information, each stage of kinking was characterized by both an image-quality map (Fig. 9) and an inverse-pole figure (Fig. 10). As noted earlier, image-quality maps are similar to conventional SEM images (with the difference that the β phase appears dark) and thus can serve as a reference in the present discussion. Inverse-pole-figure maps, on the other hand, convey detailed crystallographic information and thus are useful for in-depth insight into microstructure development. In the inverse-pole-figure maps presented here, individual α grains are colored according their crystallographic orientation relative to the radial direction, the β phase appears black; and low- and high-angle boundaries in the α phase are depicted with white and black lines, respectively.

The early stage of the kinking process is shown in Figs. 9a and 10a. At this stage, the β layers had a zigzag appearance (e.g., circled area in Fig. 9a). A close inspection (e.g., circled area in Fig. 10a) showed that such zigzag patterns resulted from shear bands extending over long distances within an α colony; these shear bands crossed both the alpha laths and β layers. The variation of orientation color indicated that material on either side of the shear bands experienced a crystallographic rotation. The bands were not completely delineated by low-angle boundaries; thus, some boundary segments probably had misorientations lower than the resolution limit of EBSD.

As the kinks became sharper (Fig. 9b), the shear bands became more pronounced and were more fully outlined by low-angle boundaries (Fig. 10b); moreover, some boundary segments had accumulated a high-angle misorientation (e.g., region circled in Fig. 10b). The progressive development of the shear bands continued during the kinking process, and, in

severely kinked α colonies (Fig. 9c), the bands were completely delineated by high-angle grain boundaries (Fig. 10c). The development of the shear bands within a kinked α colony also led to significant shearing (and break up) of the β layers (Fig. 9c) and produced a low-aspect ratio α phase grain/subgrain microstructure (Fig. 10c). Thus, the kinking process was closely linked with the development of shear bands within α colonies. Similar behavior has been noted for high-temperature deformation [5, 20]. Shear banding therefore appears to be an intrinsic feature of kinking.

It is noteworthy that there was no apparent penetration of the β phase into the α phase even in severely kinked α colonies (Figs. 1c and 9c). This observation, in conjunction with the significant level of internal stress in the α phase (deduced from Figs. 6c-d), suggests that diffusional processes were not very active. Thus, globularization during warm working was sporadic in nature in contrast to the corresponding high-temperature behavior. It may thus be concluded to arise mainly from deformation with a negligible contribution from diffusional mechanisms.

3.6. Implications for efficient warm working

Extensive microstructure observations for Ti-6Al-4V have shown that a constant strain path is the most effective method for globularizing of a colony-α microstructure *at hot-working temperatures* [22]. The present work, however, has demonstrated that that the lamellar structure is very stable during warm deformation (Figs. 7b-d); it appears that a small amount of globularization is achieved only through the kinking of α laths oriented nearly parallel to the loading direction (Fig. 10c). Statistical measurements indicated that the remaining α laths tended to be reoriented nearly perpendicular the compression direction after ~50-pct. height reduction (Fig. 2a). Hence, a change in strain path comprising rotation of the workpiece at this level of deformation may enhance the rate of globularization during warm deformation.

4. CONCLUSIONS

The EBSD technique has been employed to investigate microstructure evolution during warm working of Ti-6Al-4V alloy with a colony-α microstructure. The main conclusions from this work are as follows.

1. Microstructure evolution is driven mainly by the geometric requirements of the imposed strain and by the kinking of the α lamellae. If the angle between the α lamellae and compression direction is relatively small, the α laths are kinked. Otherwise, the α laths rotate with strain, tending to become aligned perpendicular to the loading axis, and their thickness is reduced somewhat.

2. During warm working, material flow in the α phase arises mainly from prism slip.

3. The crystallography of the transformed β microstructure is governed by the Burgers orientation relationship (OR); local crystallographic orientations of the α and β phases are related via the Burgers OR and the misorientation distribution in the α phase is dominated by the boundaries between the α variants. Plastic deformation destroys the Burgers OR between the phases and randomizes the boundaries between the α variants.

4. Warm plastic deformation is inhomogeneous within α colonies as well as within α laths. Groups of neighboring α laths are rotated with respect to each other and these rotations tend to compensate each other. It is hypothesized that this phenomenon is associated with the limited number of slip systems in α titanium which is insufficient to accommodate an arbitrary imposed strain. On the other hand, significant orientation gradients are developed along individual α laths during deformation suggesting the development of substantial internal stresses.

5. The lamellar structure is surprisingly stable during warm deformation; limited globularization is found, primarily within kinked regions. The kinking process is closely linked with development of shear bands.

6. In contrast to high-temperature deformation, a change of strain path may provide a promising method to promote globularization during warm working.

Acknowledgments

One of the authors (SM) would like to acknowledge Professor Y.S. Sato (Tohoku University, Japan) for his kind permission to carry out EBSD observations.

References

[1] Weiss I., Froes F.H., Eylon D., Welsch G.E. Metall. Trans. 1986; A17; 1935.
[2] Ari-Gur P., Semiatin S.L. Mater. Sci. Eng. 1998; A257; 118.
[3] Semiatin S.L., Seetharaman V., Weis I. Mater. Sci. Eng. 1999; A263; 257.
[4] Semiatin S.L., Bieler T.R. Acta Mater. 2001; 41; 3565.
[5] Bieler T.R., Semiatin S.L. Int. J. Plasticity 2002; 18; 1165.
[6] Kim J.H., Semiatin S.L., Lee, C.S. Acta Mater. 2003; 51; 5613.
[7] Seshacharyulu T., Medeiros S.C., Frazier W.G., Prasad Y.V.R.K. Mater. Sci. Eng. 2002; A325; 112.
[8] Zherebtsov S.V., Salishchev G.A., Galeyev R.M., Valiakhmetov O.R., Mironov S.Yu. Scripta Mater. 2004; 51; 1147.
[9] Zherebtsov S., Mazur A., Salishchev G., Lojkowski W. Mater. Sci. Eng. 2008; A485; 39.
[10] TSL OIM Version 3.0. On-line help. Draper, UT: TSL; 2001.
[11] Gundersen H.J.G., Jensen T.B. and Osterby R. J. Microscopy 1977; 113; 27.
[12] Burgers W.G. Physica 1934; 1; 561.
[13] Bhattacharyrya D., Viswanathan G.B., Denkenberger R., Furrer D., Fraser H.L. Acta Mater. 2003; 51; 4679.
[14] Gey N., Humbert M. Acta Mater. 2002; 50; 277.
[15] Wang S.C., Aindon M., Starink M.J. Acta Mater. 2003; 51; 2485.
[16] Mironov S.Yu., Salishchev G.A., Myshlyaev M.M., Pippan R. Mater. Sci. Eng. 2006; A418; 257.
[17] Hurley P.J., Humphreys F.J. Acta Mater. 2003; 51; 1087
[18] Hansen N., Juul Jensen D. Philos. Trans. R. Soc. Lond. 1999; A357; 1447.
[19] Pantleon W., Hansen N. Mater. Sci. Eng. 2001; A309; 246.
[20] Semiatin S.L., Thomas J.F., Dadras P. Metall. Trans. A 1983; 14A; 2363.

[21] Williams J.C., Baggerly R.G., Paton N.E. Metall. Mater. Trans. A, 2002; 33A; 837.
[22] Korshunov A.A., Enikeev F.U., Mazurskii M.I., Salishchev G.A., Muravlev A.V., Chistyakov P.V. Russ. Metall. 1994; 3; 103.

Table 1. Misorientation between α variants inherited from the same parent β grain [14,15]

Misorientation (Angle - Axis Pair)	Symbol	Location of Misorientation Axis on Stereographic Triangle
$60^{\circ} < 11\bar{2}0 >$	●	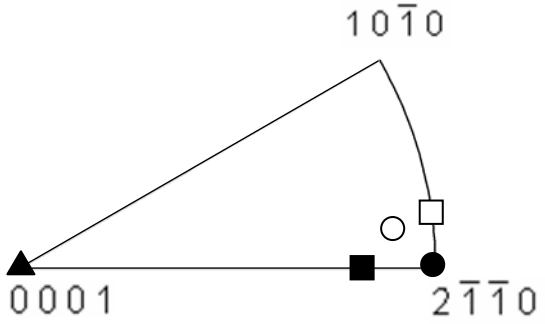
$60.8^{\circ} < \overline{1.377};\bar{1};2.377;0.359 >$	○	
$63.3^{\circ} < \overline{10};5;5;\bar{3} >$	■	
$90^{\circ} < 1;\overline{2.38};1.38;0 >$	□	
$10.5^{\circ} < 0001 >$	▲	

Figure Captions

Fig. 1. SEM images of Ti-6Al-4V microstructure (a) prior to deformation, and after height reductions of (b) 25, (c) 50, and (d) 70 pct. A high-magnification image of the microstructure is shown in the top right corner of each figure.

Fig. 2. Effect of deformation on (a) reorientation of α laths and (b) the thickness of α and β laths. Error bars show the standard deviations for the measurements.

Fig. 3. Orientation relationship between the α and β phases in Ti-6Al-4V (a) prior to deformation, and after height reductions of (b) 25 and (c) 50 pct. CD and RD denote the compression axis and radial directions, respectively.

Fig. 4. EBSD image-quality maps with highlighted boundaries linked to the Burgers orientation relationship in Ti-6Al-4V (a) prior to deformation, and after height reductions of (b) 25, (c) 50, and (d) 70 pct. The arrows indicate the locations of misorientation line scans shown in Figs. 5 and 6.

Fig. 5. Typical line scans from EBSD maps in Fig. 4 showing the variation of orientation over a long distance transverse to the α laths in Ti-6Al-4V (a) prior to deformation and after height reductions of (b) 25, (c) 50, and (d) 70 pct.

Fig. 6. Typical line scans from EBSD maps in Fig. 4 showing the variation in orientation over a long distance along the α laths in Ti-6Al-4V (a) prior to deformation, and after height reductions of (b) 25, (c) 50, and (d) 70 pct.

Fig. 7. EBSD results showing the low- and high-angle grain boundaries in the α phase (depicted as red and black lines, respectively) (a) prior to deformation, and after height reductions of (b) 25, (c) 50, and (d) 70 pct. Note that the small amount of β phase appears black in the figures.

Fig. 8. Misorientation distribution in the α phase (a) prior to deformation, and after height reductions of (b) 25, (c) 50, and (d) 70 pct. The corresponding misorientation-axis distribution is shown in the top right corner of each figure.

Fig. 9. EBSD image-quality maps illustrating the progressive development of the kinking process in α lamellae. The compression direction is vertical.

Fig. 10. EBSD inverse-pole-figure maps for radial direction illustrating the progressive development of the kinking process in α lamellae. In the maps, low- and high-angle boundaries in the α phase are depicted as white and black lines, respectively, and the β phase appears black. The compression direction is vertical.

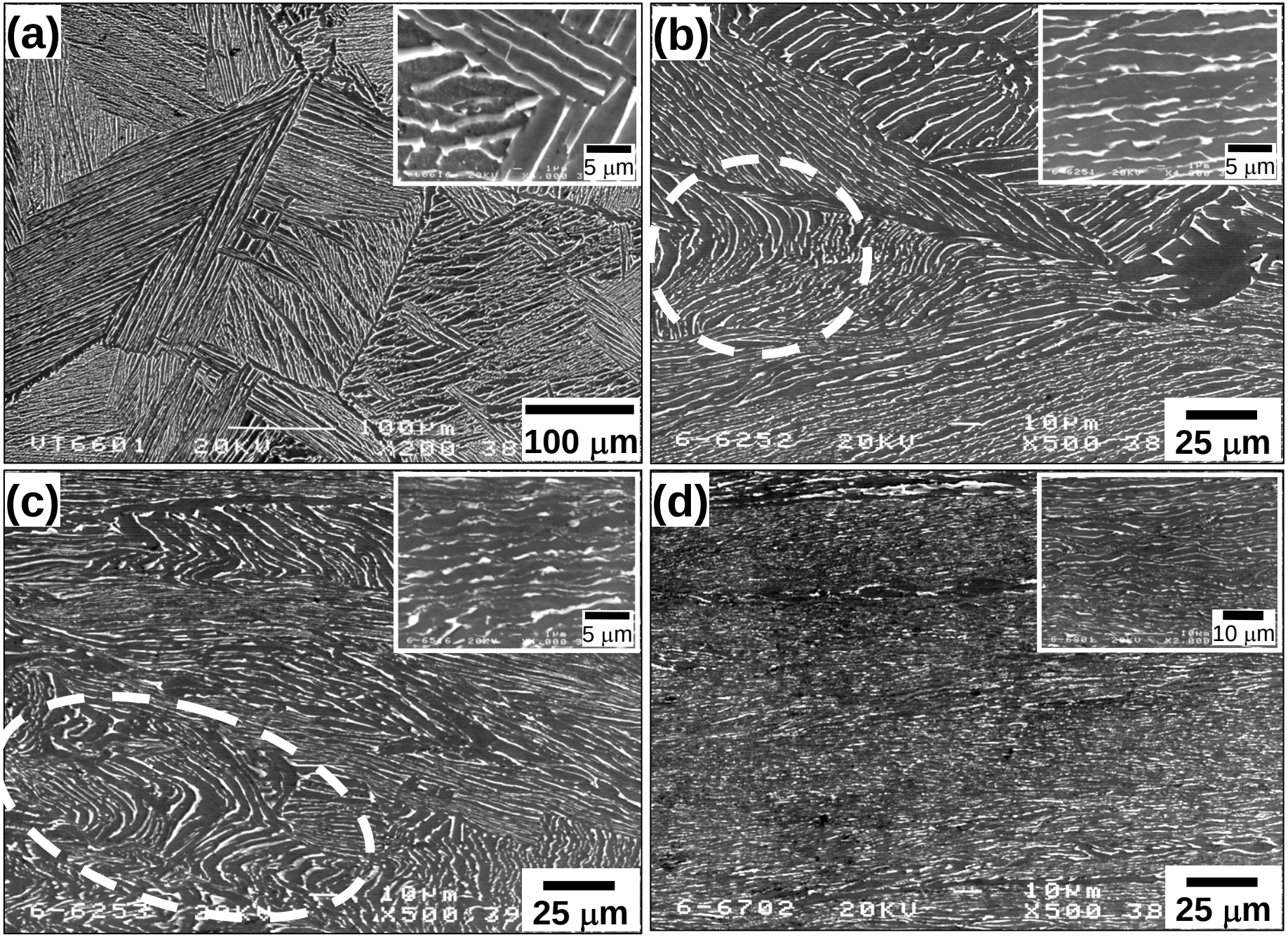

Fig. 1. SEM images of Ti-6Al-4V microstructure (a) prior to deformation, and after height reductions of (b) 25, (c) 50, and (d) 70 pct. A high-magnification image of the microstructure is shown in the top right corner of each figure. .

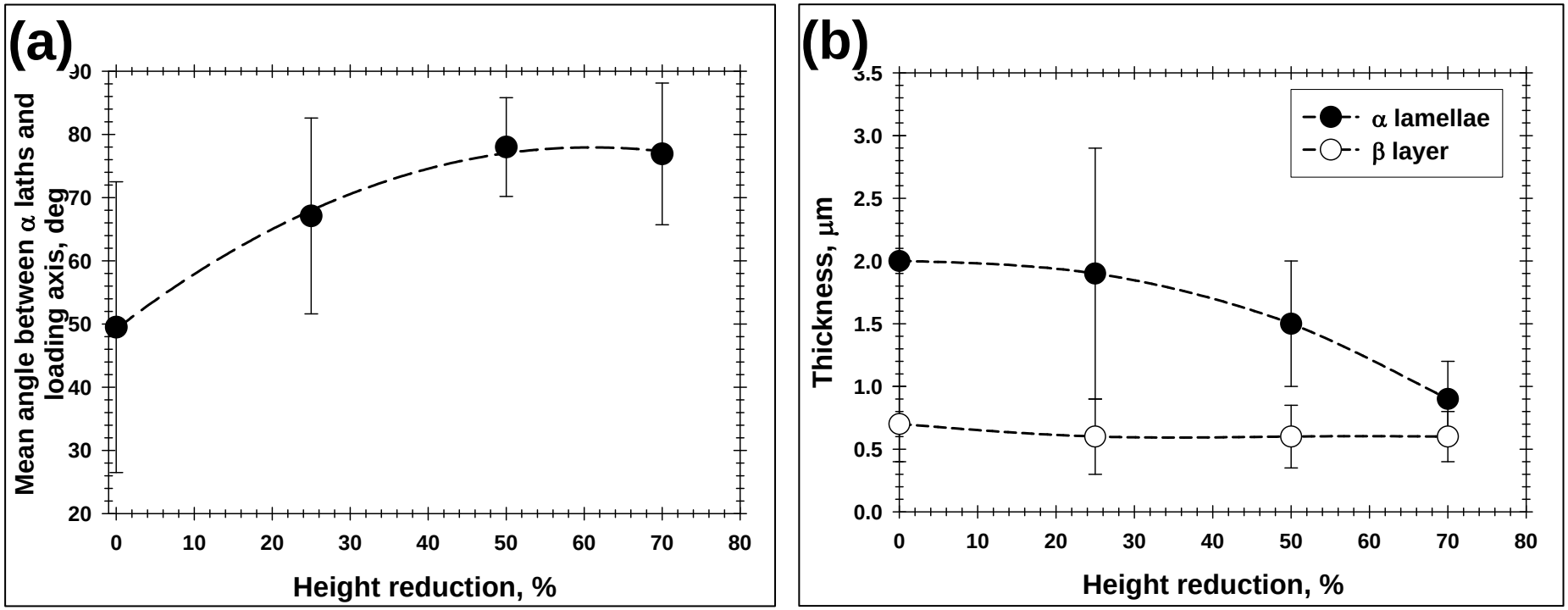

Fig. 2. Effect of deformation on (a) reorientation of α laths and (b) the thickness of α and β laths. Error bars show the standard deviations for the measurements.

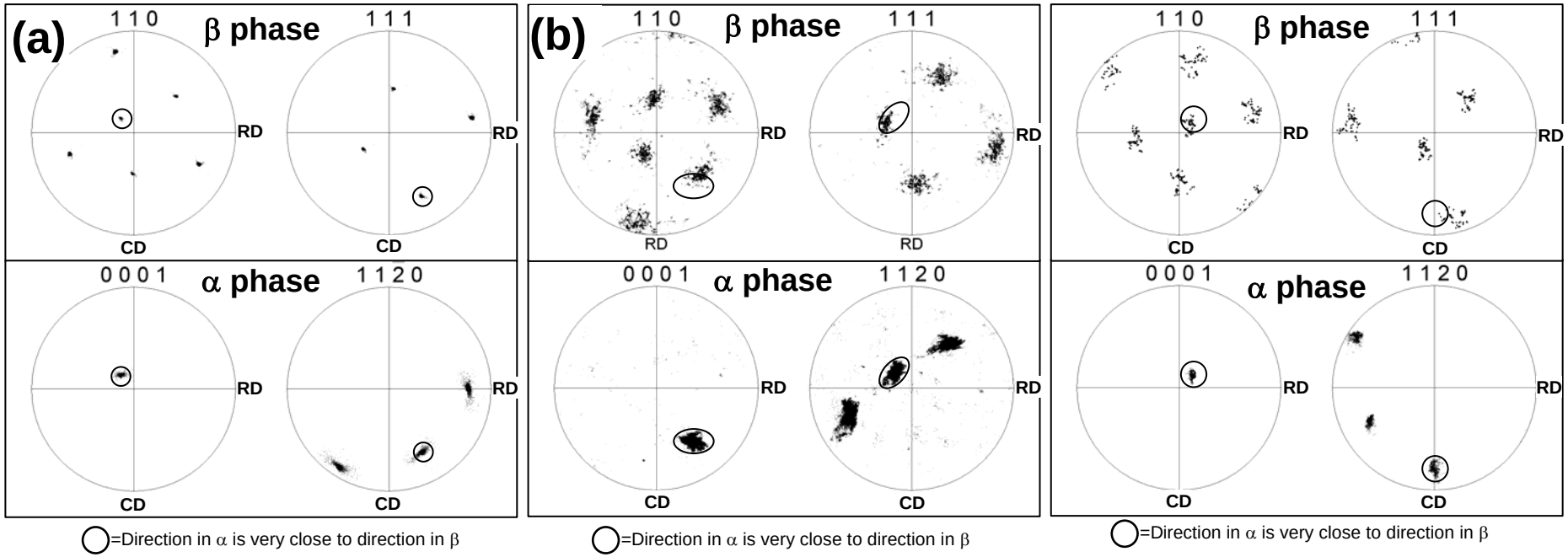

Fig. 3. Orientation relationship between the α and β phases in Ti-6Al-4V (a) prior to deformation, and after height reductions of (b) 25 and (c) 50 pct. CD and RD denote the compression axis and radial directions, respectively.

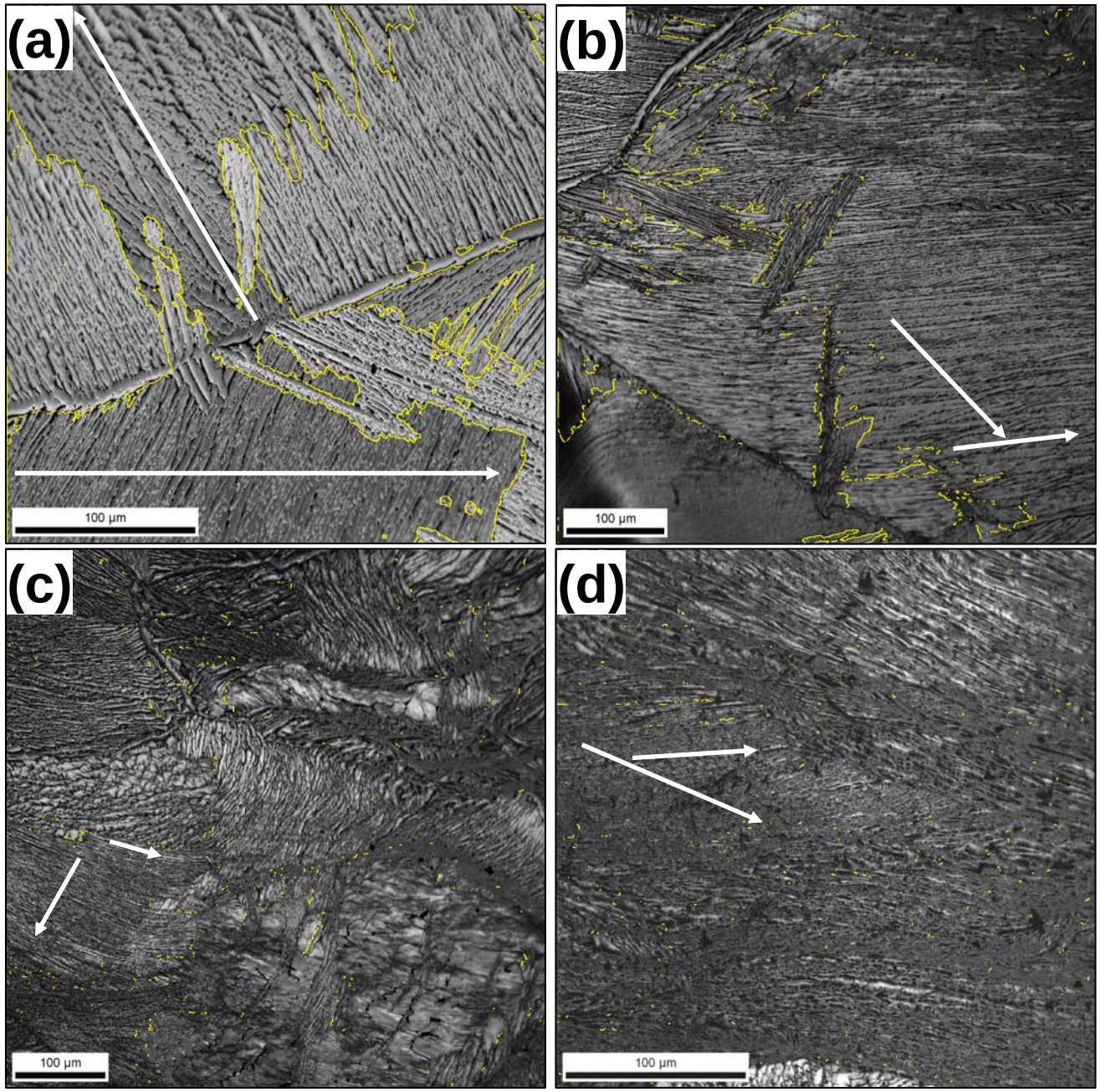

Fig. 4. EBSD image-quality maps with highlighted boundaries linked to the Burgers orientation relationship in Ti-6Al-4V (a) prior to deformation, and after height reductions of (b) 25, (c) 50, and (d) 70 pct. The arrows indicate the locations of misorientation line scans shown in Figs. 5 and 6.

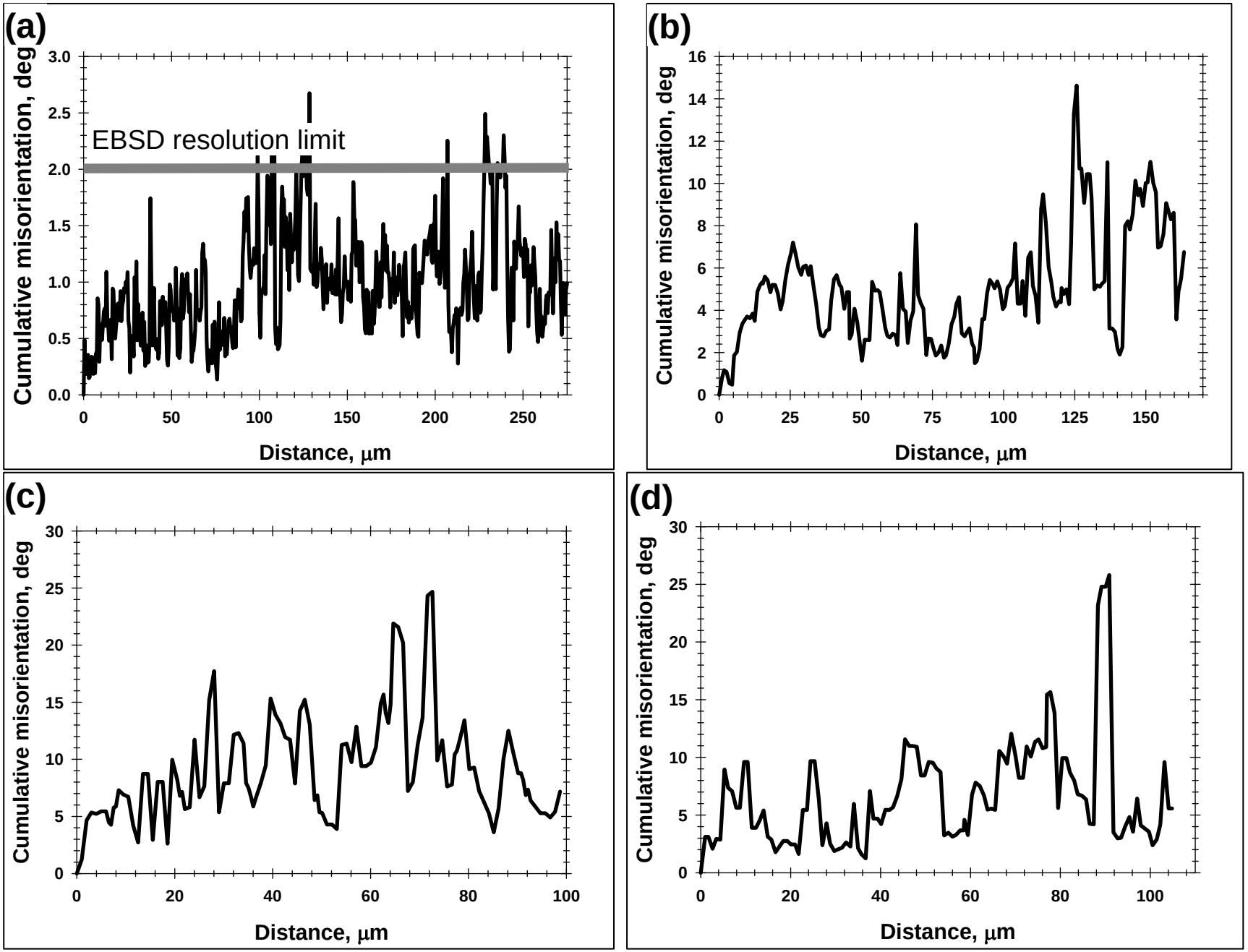

Fig. 5. Typical line scans from EBSD maps in Fig. 4 showing the variation of orientation over a long distance transverse to the α laths in Ti-6Al-4V (a) prior to deformation and after height reductions of (b) 25, (c) 50, and (d) 70 pct.

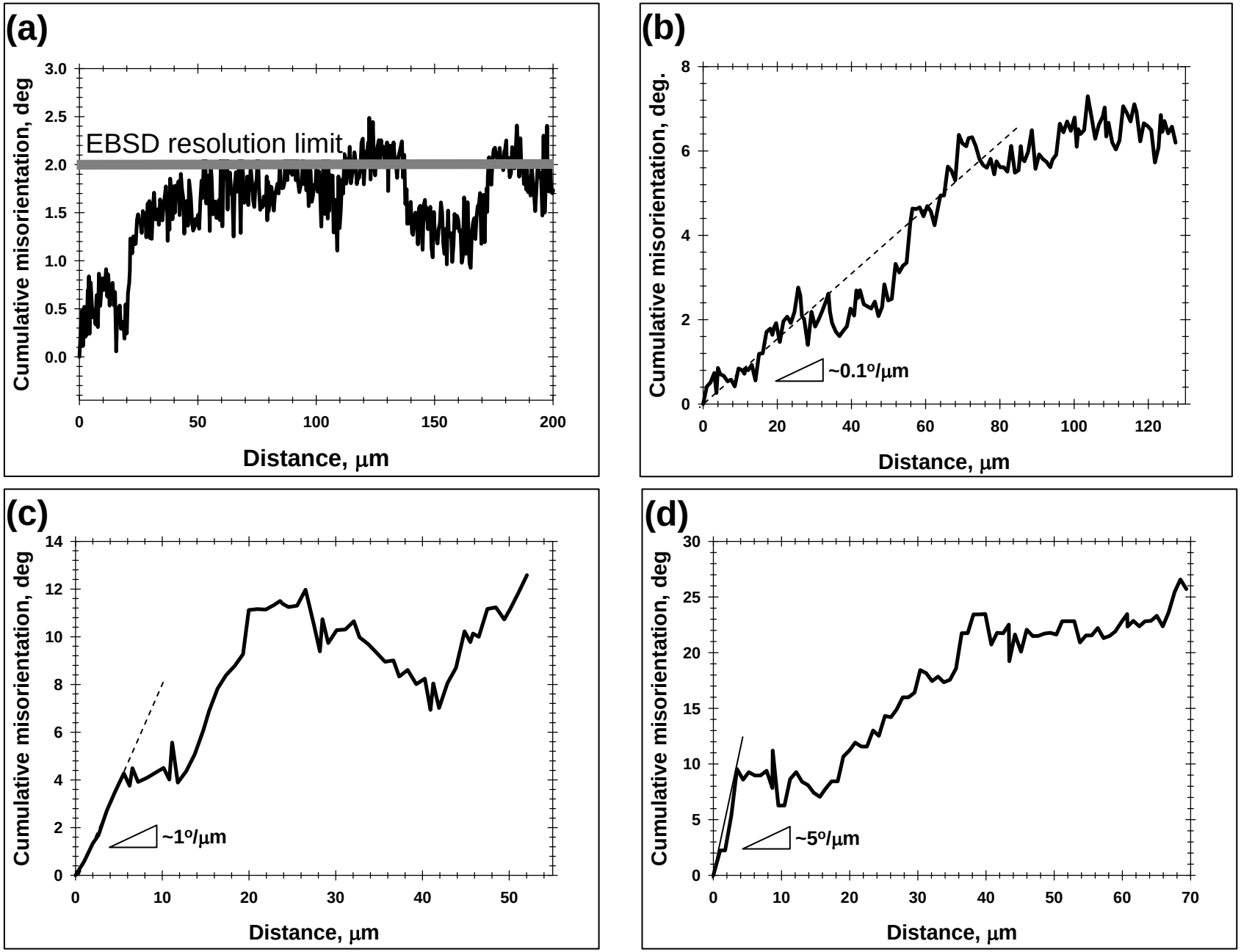

Fig. 6. Typical line scans from EBSD maps in Fig. 4 showing the variation in orientation over a long distance along the α laths in Ti-6Al-4V (a) prior to deformation, and after height reductions of (b) 25, (c) 50, and (d) 70 pct.

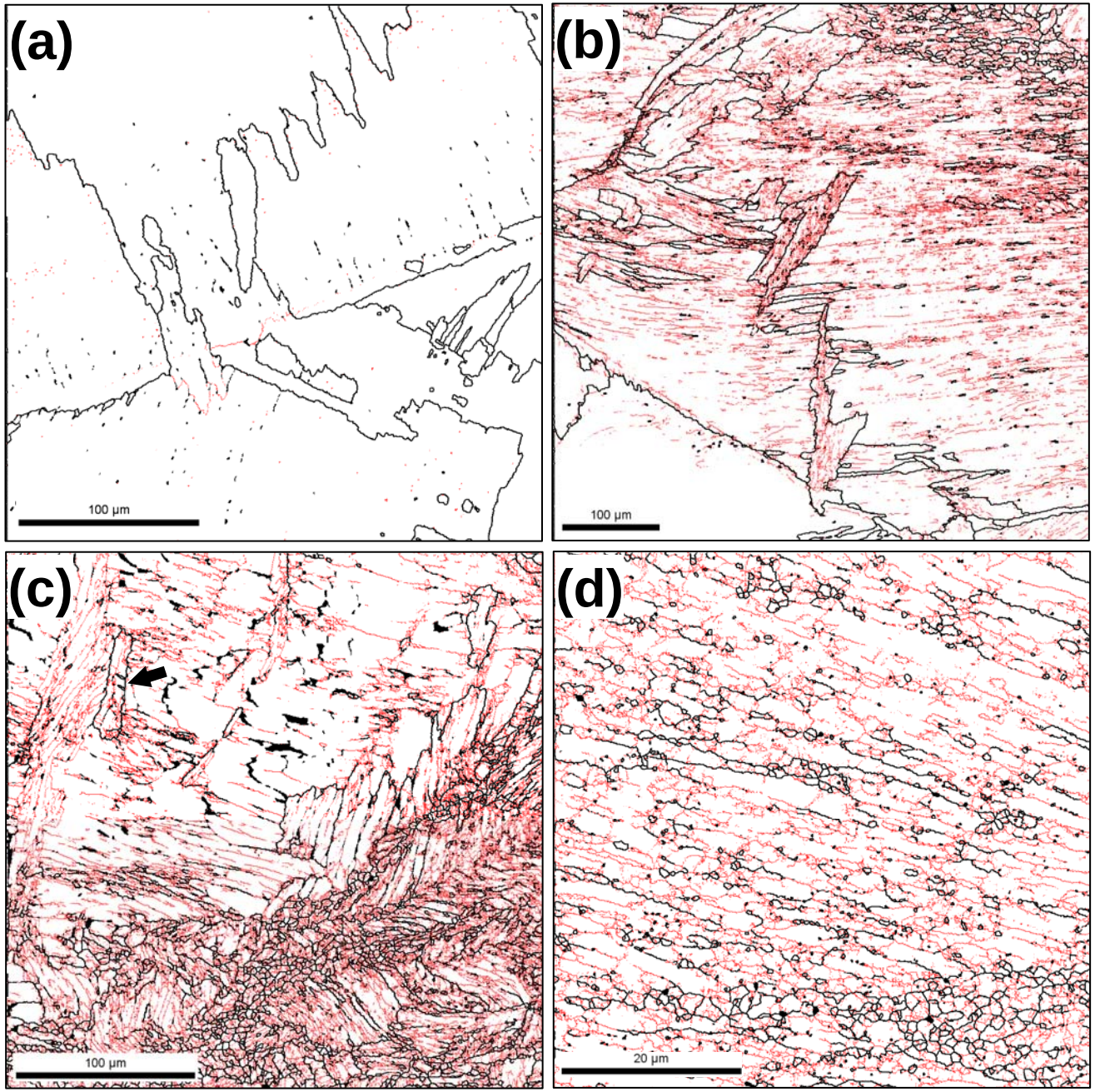

Fig. 7. EBSD results showing the low- and high-angle grain boundaries in the α phase (depicted as red and black lines, respectively) (a) prior to deformation, and after height reductions of (b) 25, (c) 50, and (d) 70 pct. Note that the small amount of β phase appears black in the figures.

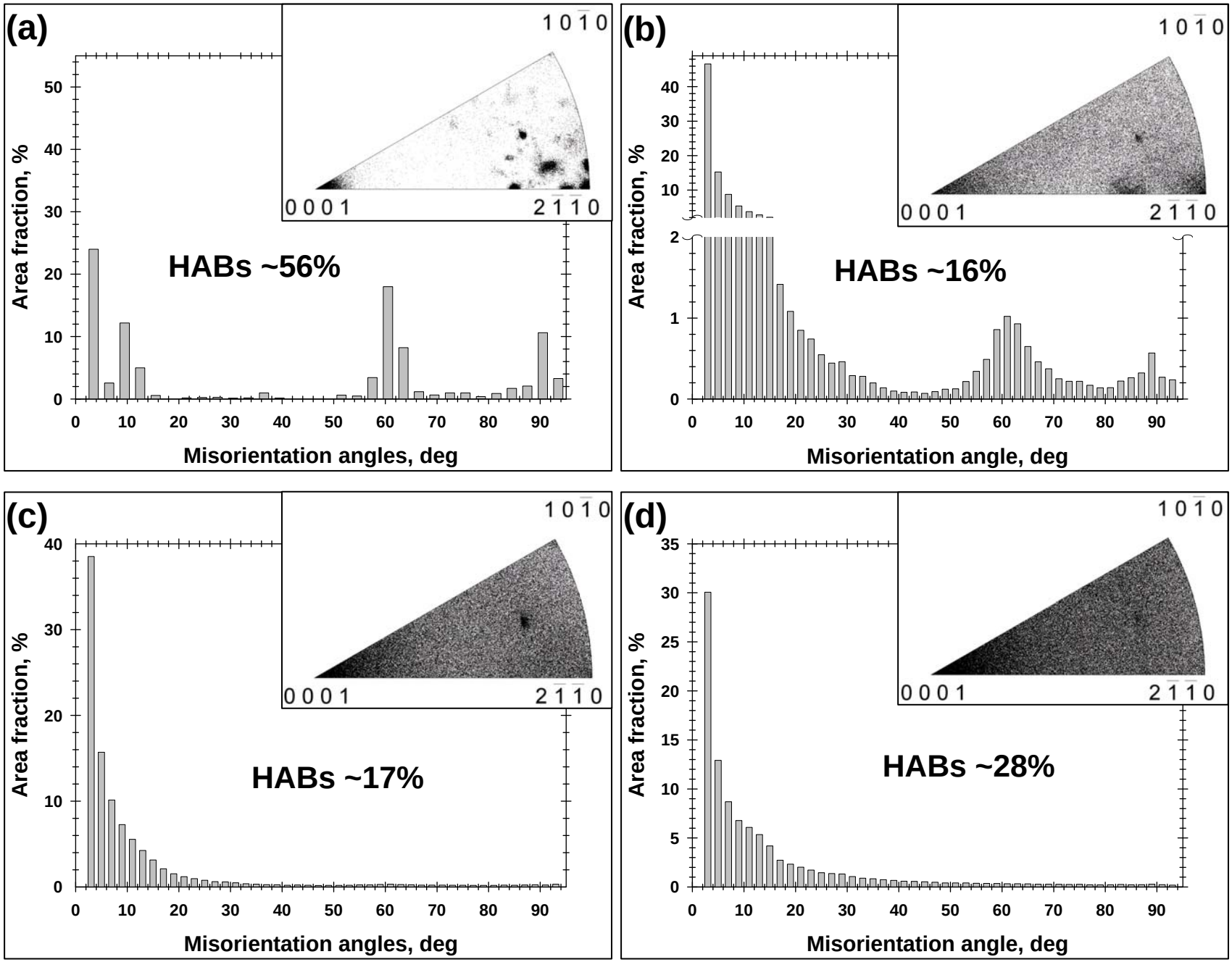

Fig. 8. Misorientation distribution in the a phase (a) prior to deformation, and after height reductions of (b) 25, (c) 50, and (d) 70 pct. The corresponding misorientation-axis distribution is shown in the top right corner of each figure.

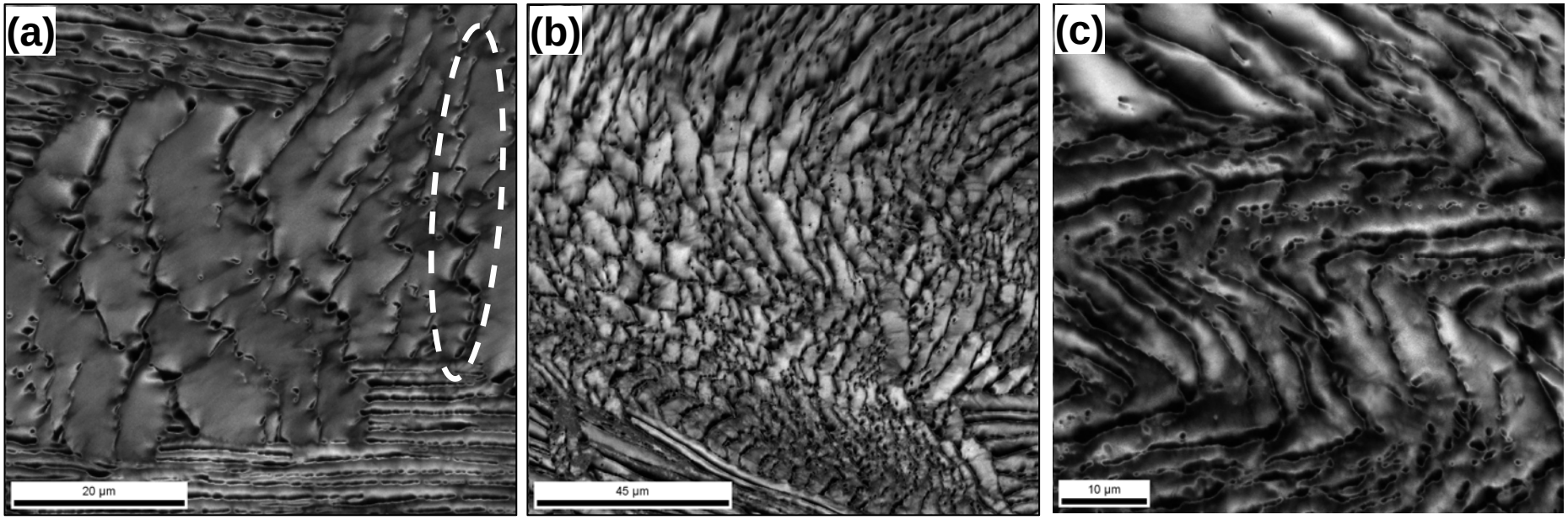

Fig. 9. EBSD image-quality maps illustrating the progressive development of the kinking process in a lamellae. Note: compression direction is vertical.

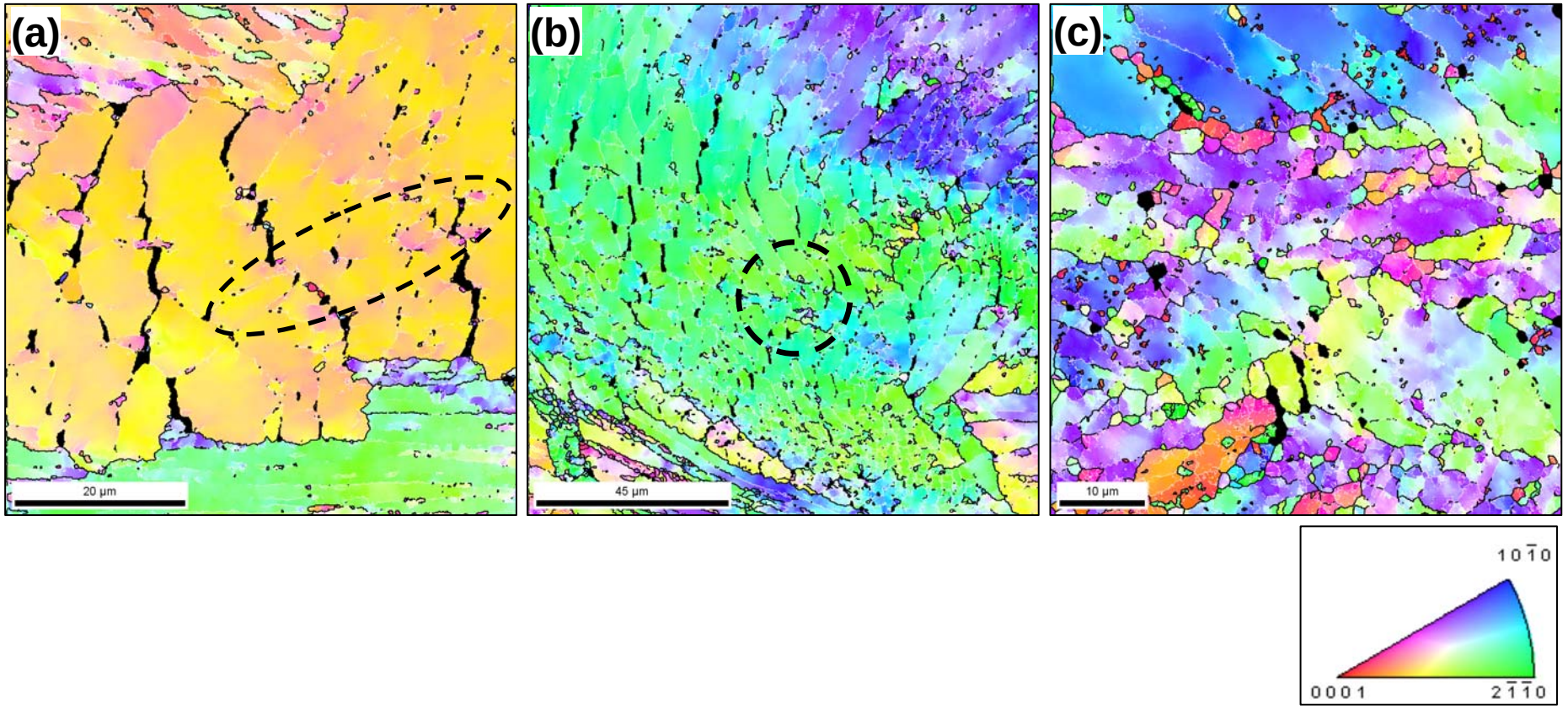

Fig. 10. EBSD inverse-pole-figure maps for radial direction illustrating the progressive development of the kinking process in α lamellae. In the maps, low- and high-angle boundaries in the α phase are depicted as white and black lines, respectively, and the β phase appears black. Color code triangle is shown in the bottom right corner. Note: compression direction is vertical